Space Weather

Supporting Information for

The development of a space climatology: 2. The distribution of power input into the magnetosphere on a 3-hourly timescale

Mike Lockwood[1], Sarah N. Bentley[1], Mathew J. Owens[1], Luke A. Barnard[1], Chris J. Scott[1], Clare E. Watt[1], Oliver Allanson[1] and Mervyn P. Freeman[2]

Paper accepted by Space Weather, October 2018.

[1]Department of Meteorology, University of Reading, Earley Gate, P.O. Box 243, Reading, Berkshire, RG6 6BB, UK

[2] British Antarctic Survey, High Cross, Madingley Road, Cambridge, CB3 0ET, UK.

Contents of this file

Introduction

Part 1

This supporting information reprises the derivation of the formula for power input into the magnetosphere P_α used in the main paper, based on the work of *Vasyliunas et al.* [1982]. This derivation was laid out in paper 1 [*Lockwood et al.*, 2018] but it is useful to repeat it here in the context of some checks carried out in parts 2 and 3 of these supporting materials.

References: Vasyliunas, V. M., J. R. Kan, G. L. Siscoe, and S.-I. Akasofu (1982) Scaling relations governing magnetospheric energy transfer, *Planet. Space Sci.*, **30**, 359–365, doi: 10.1016/00320633(82)90041-1

Lockwood, M., S. Bentley, M.J. Owens, L.A. Barnard, C.J. Scott, C.E. Watt and O. Allanson (2018b) The development of a space climatology: 1. Solar-wind magnetosphere coupling as a function of timescale and the effect of data gaps, *Space Weather*, doi: 10.1029/2018SW001856

Part 2

This part re-affirms the justification for using of the IMF magnitude *B* in the *Vasyliunas et al.* [1982] formula, rather than using the component of $\underline{B}$ transverse to the Sun-Earth line, B_T.

- This analysis uses 1-minute values of interplanetary data for 1995-2017, downloaded from the Omni2 dataset compiled and maintained by the Space Physics Data Facility, NASA/ Goddard Space Flight Center. Data available from: https://omniweb.gsfc.nasa.gov/ow_min.html
- It also employs the 3-hourly *am* geomagnetic index data compiled and maintained by L'École et Observatoire des Sciences de la Terre (EOST), a joint collaboration of the University of Strasbourg and the French National Center for Scientific Research (CNRS) and the International Service of Geomagnetic Indices (ISGI). These data are available from http://isgi.unistra.fr/data_download.php.

Part 3

This part reviews the IMF orientation factor that performs best in the P_α formulation by comparing the 1-minute interplanetary data for 1995-2017 against the 3-hourly the *am* geomagnetic index data and the 1-minute *SML* index data from the SuperMAG network.

- The *SML* data are generated by the SuperMAG network and thanks go to the contributions from Intermagnet; USGS, Jeffrey J. Love; CARISMA, PI Ian Mann; CANMOS; The S-RAMP Database, PI K. Yumoto and Dr. K. Shiokawa; The SPIDR database; AARI, PI Oleg Troshichev; The MACCS program, PI M. Engebretson, Geomagnetism Unit of the Geological Survey of Canada; GIMA; MEASURE, UCLA IGPP and Florida Institute of Technology; SAMBA, PI Eftyhia Zesta; 210 Chain, PI K. Yumoto; SAMNET, PI Farideh Honary; The institutes who maintain the IMAGE magnetometer array, PI Eija Tanskanen; PENGUIN; AUTUMN, PI Martin Connors; DTU Space, PI Dr. Rico Behlke; South Pole and McMurdo Magnetometer, PI's Louis J. Lanzarotti and Alan T. Weatherwax; ICESTAR; RAPIDMAG; PENGUIn; British Antarctic Survey; McMac, PI Dr. Peter Chi; BGS, PI Dr. Susan Macmillan; Pushkov Institute of Terrestrial Magnetism, Ionosphere and Radio Wave Propagation (IZMIRAN); GFZ, PI Dr. Juergen Matzka; MFGI, PI B. Heilig; IGFPAS, PI J. Reda; University of L'Aquila, PI M. Vellante; BCMT, V. Lesur and A. Chambodut; Data obtained in cooperation with Geoscience Australia, PI Marina Costelloe; SuperMAG, PI Jesper W. Gjerloev. The data are available from: http://supermag.jhuapl.edu/indices/?layers=SME.UL&start=2001-01-30T00%3A00%3A00.000Z&step=14400&tab=download

Part 4

This part presents two panels of Figure 8 of the main text on an enlarged scale to allows us to see, and track the evolution of, a small feature in the F_θ distribution without loss of resolution

Part 5

Gives details of the quantification of the scatter of points in each panel of Figure 1 of the main text

Part 1. Reprise of the derivation of the Vasyliunas et al. [1982] formula for energy transfer into the magnetosphere

The basis of the formula is:

$$P\alpha = \pi(L_o^2) \times (m_{sw} N_{sw} V_{sw}^3/2) \times (t_r) \quad \text{(S1)}$$

where L_o is the mean cross-sectional radius of the magnetosphere, such that the geomagnetic field presents an area πL_o^2 to the solar wind flow and ($m_{sw} N_{sw} V_{sw}^3/2$) is the kinetic energy flux of the solar wind particles (by far the dominant form of energy flux in the solar wind) , where m_{sw} is the solar wind mean ion mass, N_{sw} its number density and V_{sw} its speed. The term t_r is a dimensionless transfer function, being the fraction of the energy flux incident upon the magnetosphere that is transferred to inside the magnetosphere.

Pressure balance at the nose of the magnetosphere gives the stand-off distance to the nose of the magnetosphere, L_S [*Farrugia et al.,* 1989]

Reference: Farrugia, C.J., M.P. Freeman, S.W.H. Cowley, D.J. Southwood, M. Lockwood and A. Etemadi (1989) Pressure-driven magnetopause motions and attendant response on the ground, Planet. Space Sci., 37, 589-608, doi: 10.1016/0032-0633(89)90099-8

$$L_S = k_1 (M_E^2/P_{sw} \mu_o)^{1/6} \quad \text{(S2)}$$

Where k_1 is a geometric factor for a blunt-nosed object, M_E is Earth's magnetic dipole moment, μ_o is the magnetic constant, and P_{sw} is the solar wind dynamic pressure, given by

$$P_{sw} = m_{sw} N_{sw} V_{sw}^2 \quad (S3)$$

Vasyliunas et al. [1982] assumed the nose of the magnetosphere was hemispheric in shape, but there is no need to do this and we can define a more general shape such that

$$c_S = L_o/L_s \quad (S4)$$

Vasyliunas et al. [1982] adopted the transfer function which dimensional analysis of equation (S1) shows must be dimensionless

$$t_r = k_2 M_A^{-2\alpha} F(\theta) \quad (S5)$$

where α is the "coupling exponent" (the one free fit parameter used), $F(\theta)$ is a dimensionless function of the clock angle θ that the IMF makes with the north in the GSM frame of reference, k_2 is a constant and M_A is the Alfvén Mach number of the solar wind flow given by

$$M_A = V_{SW} (\mu_o m_{sw} N_{sw})^{1/2} / B \quad (S6)$$

Substituting equations (2) - (6) into (1) yields

$$P_\alpha = [k_1 k_2 c_S^2 \pi/(2\mu_o^{(1/3-\alpha)})] M_E^{2/3} m_{sw}^{(2/3-\alpha)} B^{2\alpha} N_{sw}^{(2/3-\alpha)} V_{sw}^{(7/3-\alpha)} F(\theta) \quad (S7)$$

If we assume the shape of the dayside magnetopause remains constant, then the shape factor c_S is constant. A survey of magnetopause crossings by *Roelof and Sibeck* [1993] demonstrated that the magnetopause response to dynamic pressure increases is largely a shape-preserving contraction and so c_S is approximately constant in these cases. On the other hand, these authors demonstrated that the response to strong southward IMF is enhanced magnetopause reconnection and erosion of the dayside (reduced L_s) and a flaring of the tail as the newly opened flux is appended to the tail (increased L_o). Hence from equation (S4) we would expect c_S to increase in substorm growth phases but then decay again in the expansion and recovery phases. At 3-hourly timescales we have some averaging over the substorm cycle, but this variable c_S could possibly become a factor on shorter timescales. If we neglect variations in c_S the term in (S7) in square brackets is constant and so is cancelled if we study P_α/P_o, where P_o is the average of P_α, taken over a long time interval. The Earth's dipole moment M_E varies on long timescales, but this can be allowed for using a model of the geomagnetic field.

Reference: Roelof, E.C. and D.G. Sibeck (1993) Magnetopause shape as a bivariate function of interplanetary magnetic field Bz and solar wind dynamic pressure. *Journal of Geophysical Research: Space Physics*, *98* (A12), pp.21421-21450, doi: 10.1029/93ja02362

Part 2. The IMF term in the Vasyliunas et al [1982] formula for energy transfer into the magnetosphere

In their paper, *Vasyliunas et al.* [1982] appear to be a little uncertain as to whether they should employ the transverse component of the IMF, B_T (the magnitude in the zy plane) or the full vector magnitude $B = (B_T^2 + B_x^2)^{1/2}$. They point out it makes only a small difference but did opt to use B_T in their text and equations. Their argument was that B_x is not relevant because the field was draped over the nose in the magnetosheath. However, this choice is somewhat inconsistent because, as shown in Part 1 of this supplementary materials file, the magnetic field enters into the coupling equation only through the Alfvén Mach number M_A in the interplanetary (unshocked) field and that depends on B and not on B_T. Previous work showed that correlations with all geomagnetic indices were consistently higher using B than for B_T and so B was employed as a result [*Lockwood et al.,* 1999] (incidentally, always at a slightly greater α value). However, this work was done with interplanetary data that contained considerable data gaps and one of the important conclusions of Paper 1 is that such gaps introduce noise. Hence it is useful to now check this conclusion still holds given we now have 20 years of data with few and only short data gaps. advantage of B over B_T could just have been due to the noise introduced by data gaps. We here use equation (S7) in Part 1 of these supplementary materials, along with the near continuous 1-minute data for 1995-2017 (inclusive). We also deploy the method laid out in paper 1 for identifying and dealing with data gaps. Specifically: there must be sufficient 1-min samples in an hour to give an hourly mean with uncertainty below 5% for each parameter; these hourly means are then combined to make hourly P_α values that are averaged into the 3-hourly intervals only when all 3 hours have a valid P_α).

Reference: Lockwood, M., R. Stamper and M.N. Wild (1999) A doubling of the sun's coronal magnetic field during the last 100 years, *Nature*, **399,** 437-439, doi: 10.1038/20867

This was done using equation (S7) as given above (and as used in the main part of the paper) with the IMF term being, in the first instance, the total field strength B. Then all calculations were repeated replacing B with B_T.

The correlations of the P_α values with the *am* index were then compared. Figure S1 shows the correlograms, giving these correlations as a function of the assumed coupling exponent, α. The solid lines employ B and dashed lines use B_T. The black lines are for simultaneous 3-hourly values. The blue lines are for annual values of P_α, $\langle P_\alpha \rangle_{\tau=1yr}$, computed by averaging 3-hourly P_α values together (the combine-then-average approach). The red lines are for $[P_\alpha]_{ann}$, that are generated from annual means of the constituent terms (the average then combine approach).

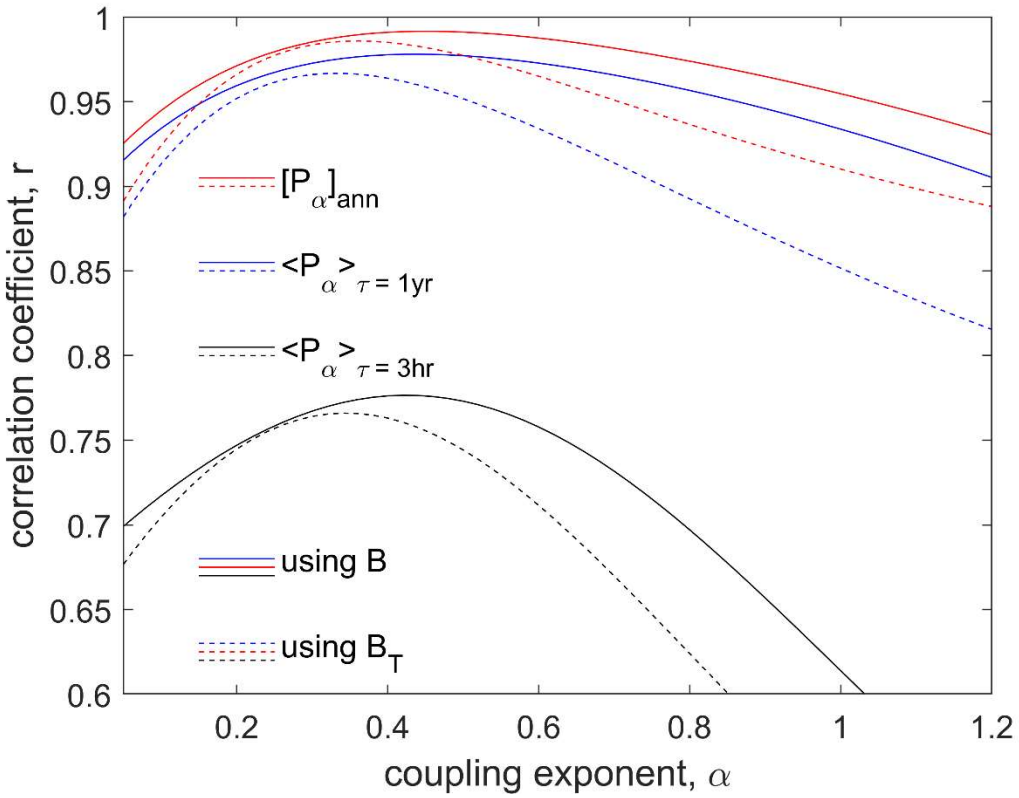

Figure S1. Analysis of the effects of using the IMF magnitude B and its transverse component $B_T = (B_{YM}^2 + B_{ZM}^2)^{1/2}$ in computing the power input to the magnetosphere P_α. The plots are correlograms showing the correlation coefficient between simultaneous values of P_α as a function of the coupling exponent, α, and solid lines use B and dashed lines use B_T. The black lines are for simultaneous 3-hourly values. The blue lines are for annual values, where annual values of P_α are $\langle P_\alpha \rangle_{\tau=1yr}$, computed by averaging 3-hourly P_α values together (the combine-then-average approach). The red lines are for $[P_\alpha]_{ann}$, that are generated from annual means of the constituent terms (the average then combine approach).

It can be seen that in all three cases, B gives slightly higher peak correlations than B_T (but always at a slightly higher value of α). This confirms the use of B in the main paper is slightly better than using B_T.

Part 3. The IMF orientation term $F(\theta)$ of the Vasyliunas et al. [1982] formula for energy transfer into the magnetosphere

In their paper, *Vasyliunas et al.* [1982] do not specify a form for $F(\theta)$, other than noting it must be dimensionless. These authors do, however, specify the best way to identify the optimum $F(\theta)$, which we do deploy here, although we note that there are pitfalls that have to be avoided. As in the main text we express equation (S7) as

$$P_\alpha = (k_3 M_E^{2/3})\, F_B\, F_V\, F_N\, F_\theta \qquad \text{(S8)}$$

where $F_B = B^{2\alpha}$, $F_V = V_{sw}^{(7/3-\alpha)}$ and $F_N = (m_{sw}\, N_{sw})^{(2/3-\alpha)}$. We also further combine the product of three terms into a $G_\alpha = F_B.F_V.F_N$ so that

$$P_\alpha = (k_3 M_E^{2/3})\, G_\alpha\, F_\theta \qquad \text{and hence} \qquad \text{(S9)}$$

$$P_\alpha/P_o = (k_3 M_E^{2/3})\, G_\alpha\, F_\theta \,/\langle (k_3 M_E^{2/3})\, G_\alpha\, F_\theta \rangle = G_\alpha\, F_\theta \,/\langle G_\alpha\, F_\theta \rangle = G\, F_\theta \,/\, G_o \qquad \text{(S10)}$$

Where the average is taken over all data and $G_o = \langle G_\alpha F_\theta \rangle$. As the ideal coupling function P_α/P_o would be proportional to the geomagnetic index (we here use the *am* index in the first instance), in which case from (S10) $am/(G/G_o)$ would be proportional to F_θ. This is the method *Vasyliunas et al.* [1982] proposed to evaluate a potential IMF orientation functions F_θ.

As discussed in the main text, a number forms for F_θ have been proposed. We here test $F_\theta = \sin^n(\theta/2)$ for n of 2, 3, 4, and 5 and also the so-called "half-wave rectifier" function $F_\theta = U(\theta)\cos(\theta)$, where $U(\theta) = -1$ for $\theta \geq 90^o$ and $U(\theta) = 0$ for $\theta < 90^o$. The observed (3 hourly) F_θ values for each tested functional form are binned into 20 bins of F_θ that are 0.05 wide and the mean values of the ratio $am/(G/G_o)$ evaluated for each bin. Figure S2 shows these means for $n = 2$ as black points. The error bars are plus and minus one standard deviation and show that there is great scatter. The means are fitted with a least squares linear regression (in figure S2 the orange line) and the goodness-of-fit quantified using the root-mean-square (r.m.s.) fit residual Δ_{rms}. For $n = 2$, $\Delta_{rms} = 0.081$nT which is relatively large, consistent with the fact that the variation of the means of the ratio is not close to a linear variation with F_θ.

Figure S3 shows the corresponding results for $n = 3$ which yields an r.m.s. fit residual $\Delta_{rms} = 0.030$nT. Hence the linear fit for $\sin^3(\theta/2)$ (the cyan line) is better than for $\sin^2(\theta/2)$. Figure S4 shows the corresponding results for $n = 4$ which yields a yet lower r.m.s. fit residual $\Delta_{rms} = 0.021$nT. Hence the linear fit for $\sin^4(\theta/2)$ (the cyan line) is better again. Figure S5 shows the corresponding results for $n = 5$ which yields a slightly larger (than for $n = 4$) r.m.s. fit residual $\Delta_{rms} = 0.039$nT: hence the linear fit (mauve line) is a less good fit than for $\sin^4(\theta/2)$. Lastly Figure S6 is for $F_\theta = U(\theta)\cos(\theta)$ and gives $\Delta_{rms} = 0.037$nT, hence the linear fit (the black line) is quite good for $U(\theta)\cos(\theta)$, but figure S6 shows the point for lowest bin ($0 \geq F_\theta > 0.05$) is notably further from the fitted line than for other bins. This is significant because this bin contains all zero values of F_θ which, it must be remembered, is half the data set for this form of F_θ (all data at times when $B_{ZM} > 0$).

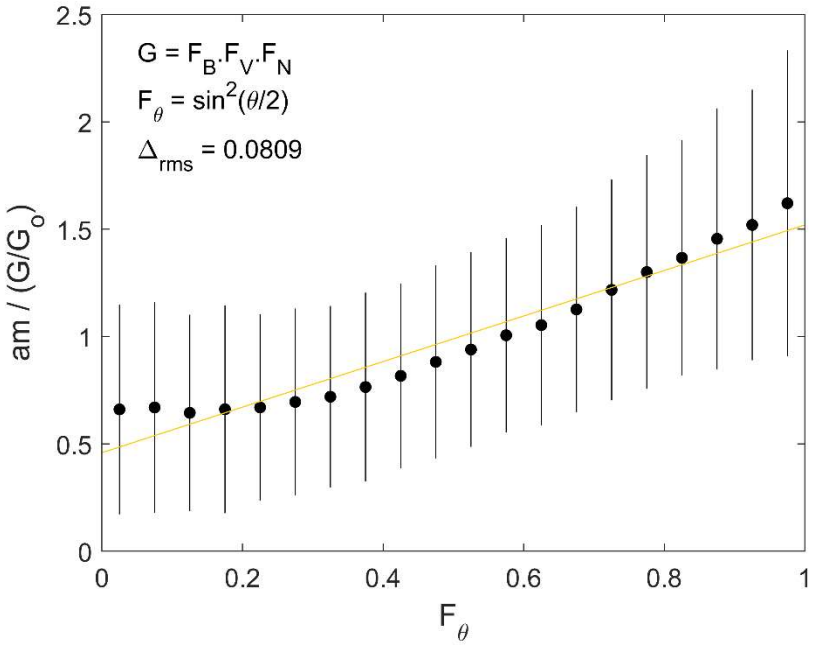

Figure S2. Analysis of IMF orientation factor $F_\theta = \sin^2(\theta/2)$ **,** i.e. $n = 2$. The 3-hourly IMF data for 1995-2017 are binned into 20 bins of observed $F(\theta)$ that are 0.05 wide. The points are the mean of the ratio $am/(G/G_o)$ for each bin where $G = F_B.F_V.F_N$ and G_o is the average of GF_θ for all data. The error bars are plus and minus one standard deviation. These points would lie along a straight line for an ideal coupling function and the orange line is the best linear regression fit to the means. The closeness of fit is quantified by the r.m.s. fit residual Δ_{rms} = 0.081nT.

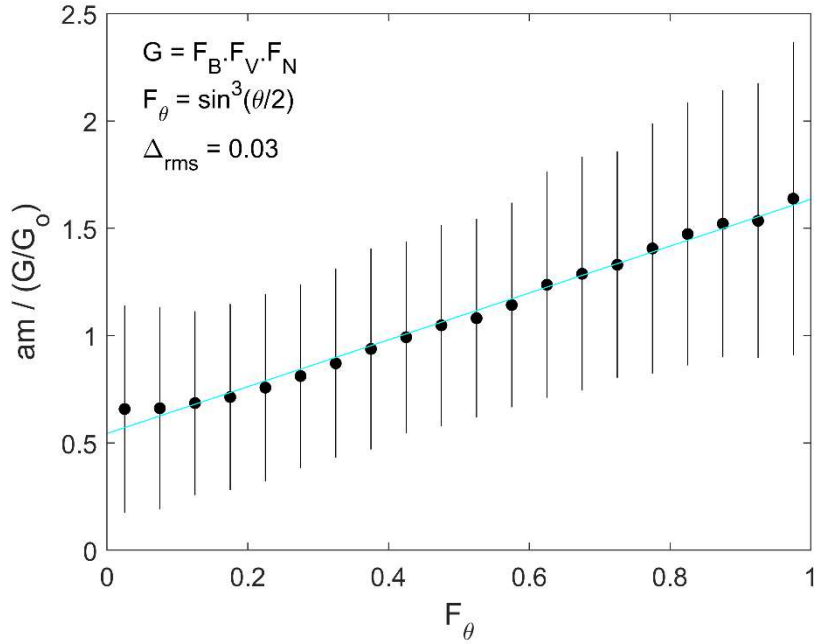

Figure S3. Same as Figure S2 for IMF orientation factor $F_\theta = \sin^3(\theta/2)$ **,** i.e. $n = 3$. The r.m.s. fit residual Δ_{rms} = 0.030nT.

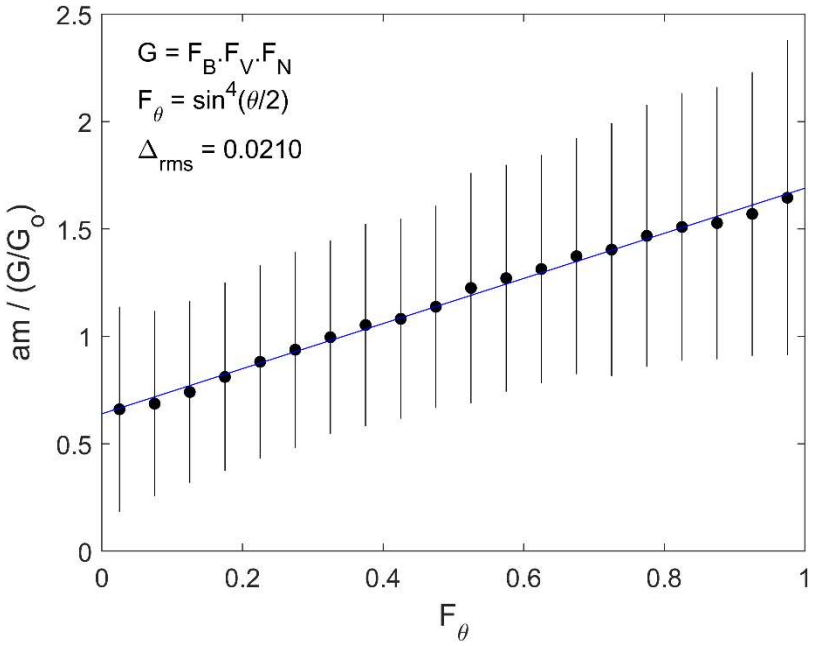

Figure S4. Same as Figure S2 for IMF orientation factor $F_\theta = \sin^4(\theta/2)$, i.e. $n = 4$. The r.m.s. fit residual Δ_{rms} = 0.021nT.

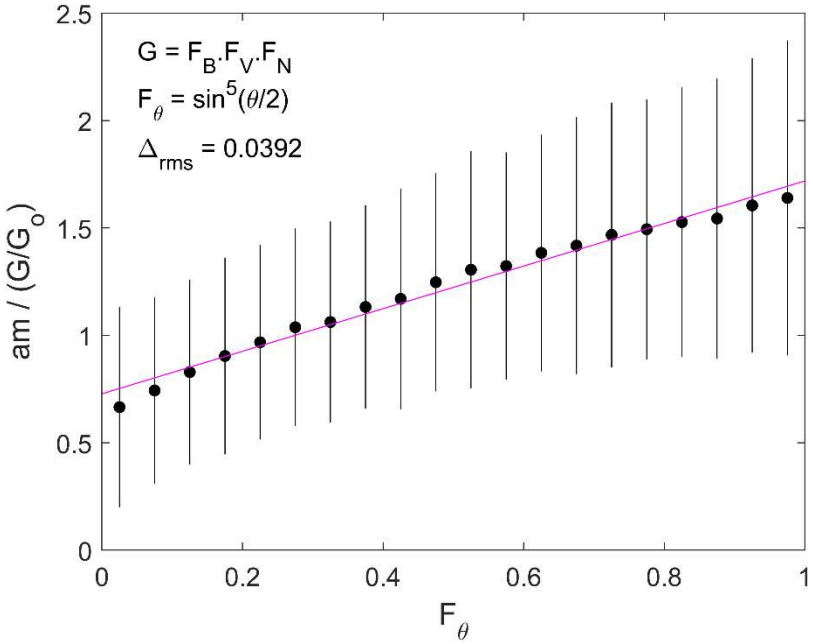

Figure S5. Same as Figure S2 for IMF orientation factor $F_\theta = \sin^5(\theta/2)$, i.e. $n = 5$. The r.m.s. fit residual Δ_{rms} = 0.039nT.

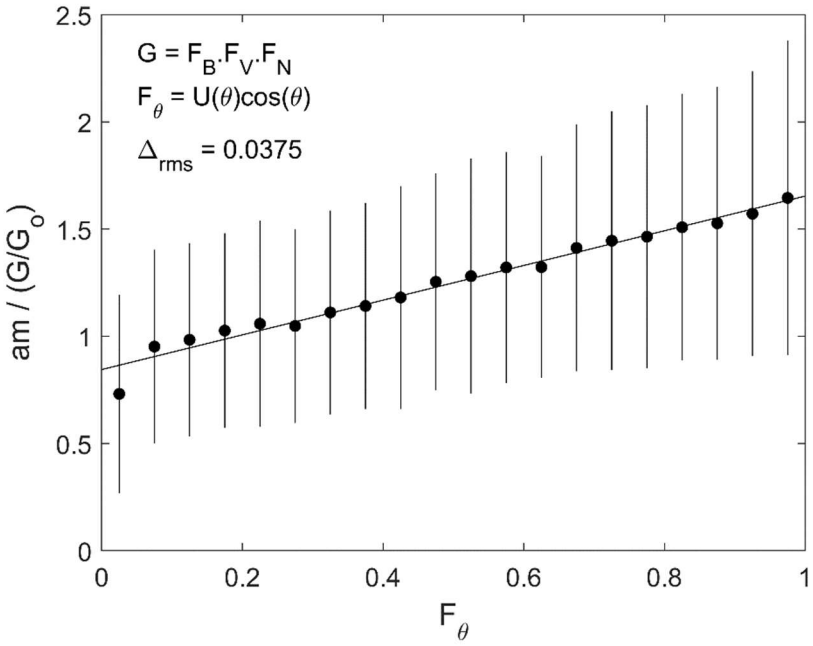

Figure S6. Same as Figure S2 for IMF orientation factor $F_\theta = U(\theta)\cos(\theta)$, where $U(\theta) = -1$ for $\theta \geq 90^o$ and $U(\theta) = 0$ for $\theta < 90^o$. The r.m.s. fit residual $\Delta_{rms} = 0.037$nT.

This procedure was repeated for one-minute resolution data. The geomagnetic index used *SML*, the equivalent of the *AL* index that monitors the auroral electrojet, but derived from the much more extensive SuperMAG network of magnetometers. The interplanetary data are lagged by 36 min., the lag of peak correlation of the response in *SML*, corresponding to the average length of the substorm growth phase, as found in Paper 1 [*Lockwood et al.*, 2018]. Figures S7-S11 are the corresponding plots to S2-S6 for these 1-minute interplanetary data and one-minute *SML* data. Because *SML* is increasingly negative as disturbance levels increase the ratio $SML/(G/G_o)$ is negative and become increasingly negative as F_θ increases. The minimum fit residual Δ_{rms} is again for $F_\theta = \sin^4(\theta/2)$. $F_\theta = U(\theta)\cos(\theta)$ again performed quite well, but the lowest bin is again not well fitted, which is significant because it contains over half the total number of samples for this form of F_θ.

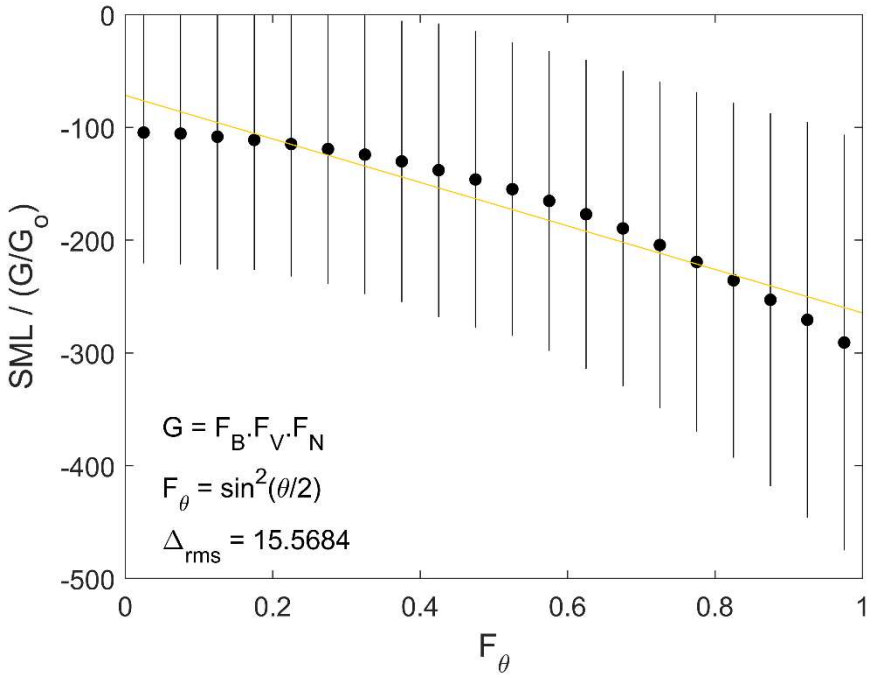

Figure S7. Analysis of IMF orientation factor $F_\theta = \sin^2(\theta/2)$, i.e. $n = 2$. The 1-minute IMF data for 1995-2017 are binned into 20 bins of observed $F(\theta)$ that are 0.05 wide. The points are the mean of the ratio $SML/(G/G_o)$ for each bin where $G = F_B.F_V.F_N$ and G_o is the overall average of GF_θ for all data. The error bars are plus and minus one standard deviation. These points should lie along a straight line for the ideal coupling function and the mauve line is the best linear regression fit to the means. The closeness of fit is quantified by the r.m.s. fit residual Δ_{rms}, which is this case is 15.57nT.

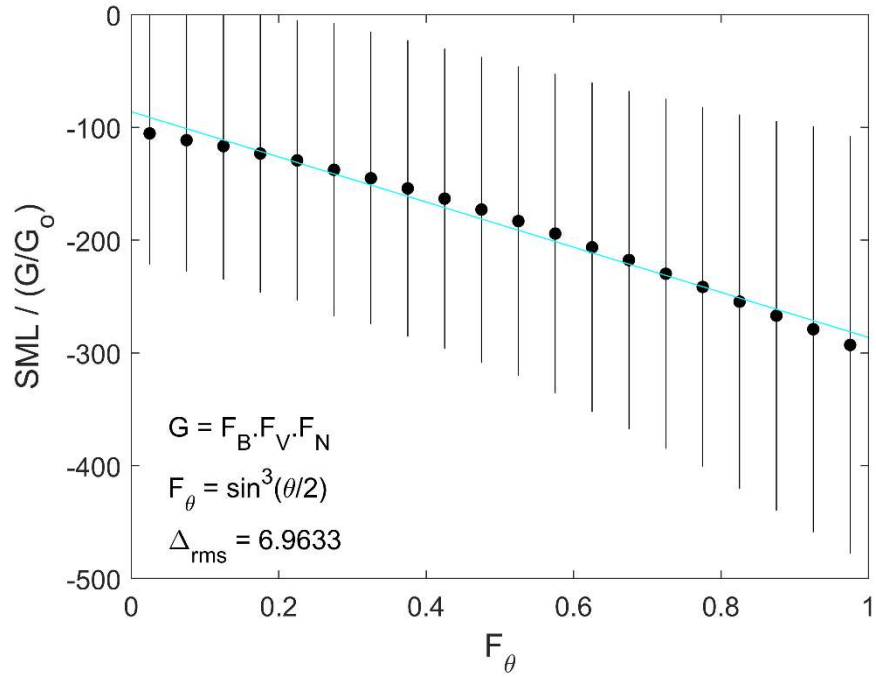

Figure S8. Same as Figure S7 for IMF orientation factor $F_\theta = \sin^3(\theta/2)$, i.e. $n = 3$. The r.m.s. fit residual $\Delta_{rms} = 6.96$nT.

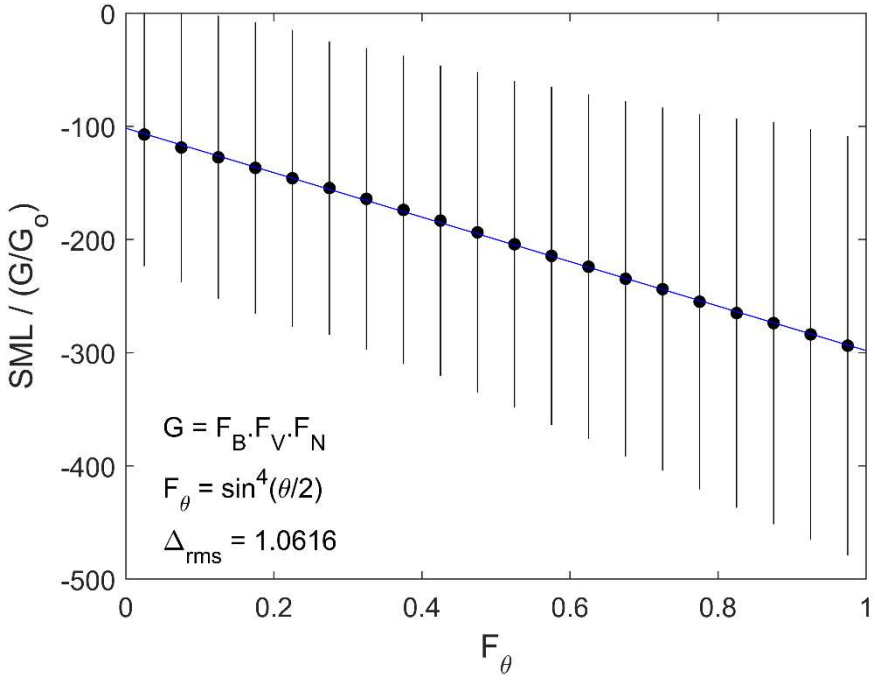

Figure S9. Same as Figure S7 for IMF orientation factor $F_\theta = \sin^4(\theta/2)$, i.e. $n = 4$. The r.m.s. fit residual Δ_{rms} = 1.06 nT.

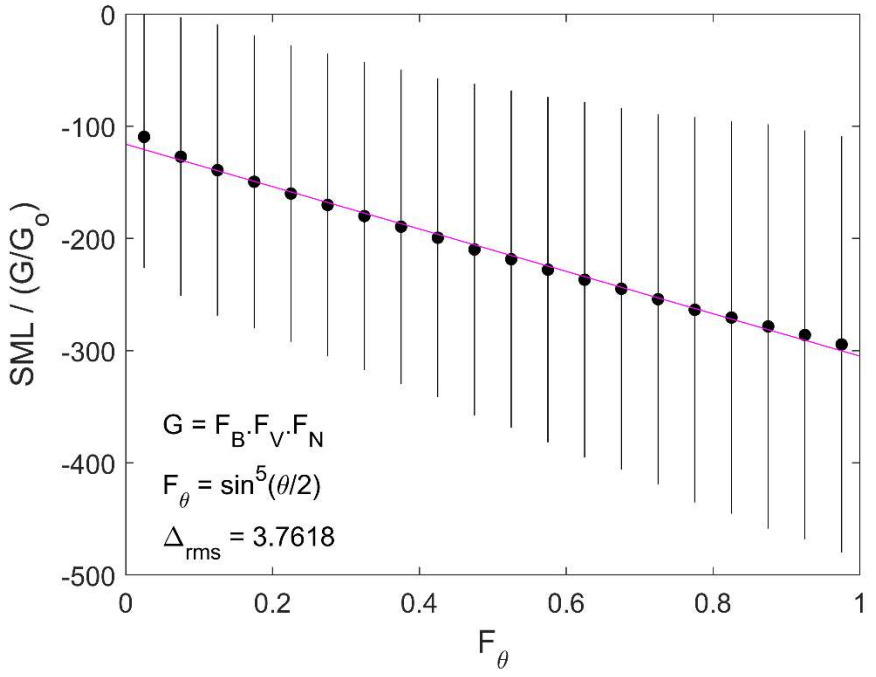

Figure S10. Same as Figure S7 for IMF orientation factor $F_\theta = \sin^5(\theta/2)$, i.e. $n = 5$. The r.m.s. fit residual Δ_{rms} = 3.76nT.

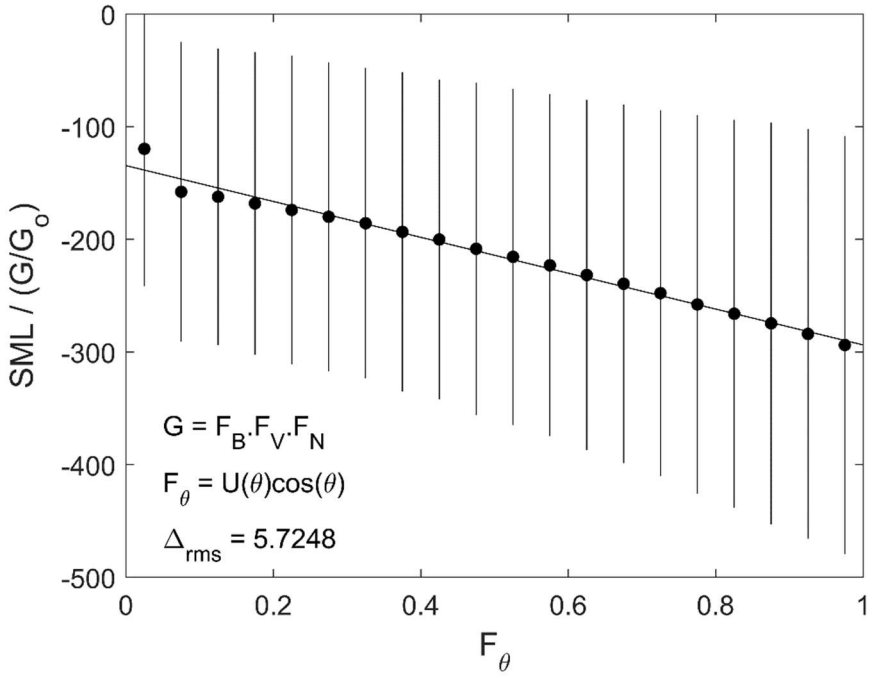

Figure S11. Same as Figure S7 for IMF orientation factor $F_\theta = U(\theta)\cos(\theta)$, where $U(\theta) = -1$ for $\theta \geq 90^o$ and $U(\theta) = 0$ for $\theta < 90^o$. The r.m.s. fit residual $\Delta_{rms} = 5.72$nT.

Figures S12 and S13 take 2 different looks at the fits for 1-minute *SML* data. In these plots the data have been binned into 20 bins of the clock angle θ, rather than in F_θ. Figure 12 is of a format used by *Wygant et al*., (1983), *Bargatze et al.* (1986) and *Newell et al.* (2017). The plot shows the 5 forms of F_θ tested here namely:, (orange) $\sin^2(\theta/2)$; (cyan) $\sin^3(\theta/2)$; (blue) $\sin^4(\theta/2)$; (mauve) $\sin^5(\theta/2)$; and (black) $U(\theta)\cos(\theta)$, each as a function of θ. The black points are the observed values of $SML/(G/G0)$, scaled to vary between zero and unity (to match the values of F_θ), $s[SML/(G/G0),]+c$, as employed by *Bargatze et al (*1986), and *Newell et al.* (2007). Note than because *SML* is negative, *s* is also negative. A big difference between Figure S12 (and Figure S13) and Figures S7-S11 is in the distribution of numbers of samples in each bin because the bins in S12 and S13 are of fixed width in θ whereas in S7-S11 they were of fixed width in F_θ. It can be seen that the best fit, as expected from Figures 7-11, is $\sin^4(\theta/2)$, but the "half-wave rectified" form $U(\theta)\cos(\theta)$ does not appear to perform too badly. However, Figure 13 shows how the plot format has helped disguise a serious problem with this form for F_θ.

In Figure S13 the data (the black points) are plotted unscaled, i.e. $-SML/(G/G0)$ (where the minus sign is included because *SML* is negative). In this case the various forms of F_θ are individually fitted to the data using the coefficients of the respective linear fit, as show in Figures S7-S11. Again $F_\theta = \sin^4(\theta/2)$ is an excellent fit to the data and better than all the others.

In this plot $F_\theta = U(\theta)\cos(\theta)$ does not look a good fit, the point being that all points at $\theta < 90^o$ in Figure S13 appear only in the lowest bin in Figure S11, because for all such points F_θ is zero for $U(\theta)\cos(\theta)$.

We conclude that by far the best form of the dimensionless IMF orientation factor F_θ is in the expressions for power input to the magnetosphere P_α is $\sin^4(\theta/2)$. This has been shown to be true for 1-minute values and for 3-hourly means.

References: Wygant, J. R., R. B. Torbert, and F. S. Mozer (1983) Comparison of S3-3 polar cap potential drops with the interplanetary magnetic field and models of magnetopause reconnection, *J. Geophys. Res.*, **88** (A7), 5727–5735, doi: 10.1029/JA088iA07p05727.

Bargatze, L.F.B., R. L. McPherron, D. N. Baker (1986) Solar Wind-Magnetosphere Energy Input Functions, in *Solar Wind-Magnetosphere Coupling*. Eds, Y. Kamide, J.A. Slavin, Terra Scientific Publishing Company, Tokyo, Japan, and D. Reidel Publishing Company, Dordrecht, Holland, ISBN: 90-277-2303-6, pp. 101-109, doi: 10.1007/978-94-009-4722-1_7.

Newell, P.T., T. Sotirelis, K. Liou, C.-I. Meng, and F. J. Rich (2007) A nearly universal solar wind-magnetosphere coupling function inferred from 10 magnetospheric state variables, *J. Geophys. Res.*, **112**, A01206, doi:10.1029/2006JA012015

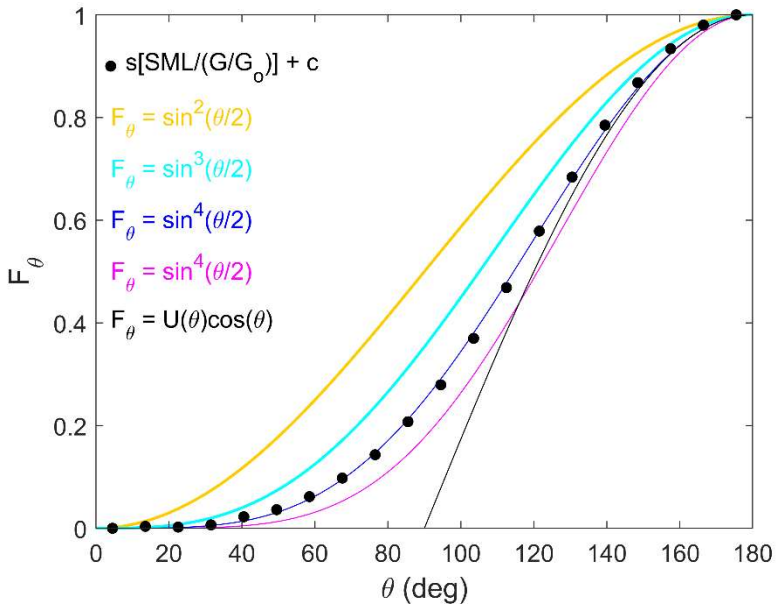

Figure S12. Same fits shown in figures S7 –S11 bit shown on a F_θ-θ axes. The data (black points) are means of the ratio *SML*/(*G*/*G*o), linearly scaled to vary between 0 and 1, *s*[*SML*/(*G*/*G*o)]+*c*. (Note that *s* is negative because SML values are negative). The means are taken in 20 bins of θ, each 9° wide. The F_θ functions shown are: (orange) $\sin^2(\theta/2)$; (cyan) $\sin^3(\theta/2)$; (blue) $\sin^4(\theta/2)$; (mauve) $\sin^5(\theta/2)$; and (black) $U(\theta)\cos(\theta)$, where $U(\theta) = -1$ for $\theta \geq 90^o$ and $U(\theta) = 0$ for $\theta < 90^o$.

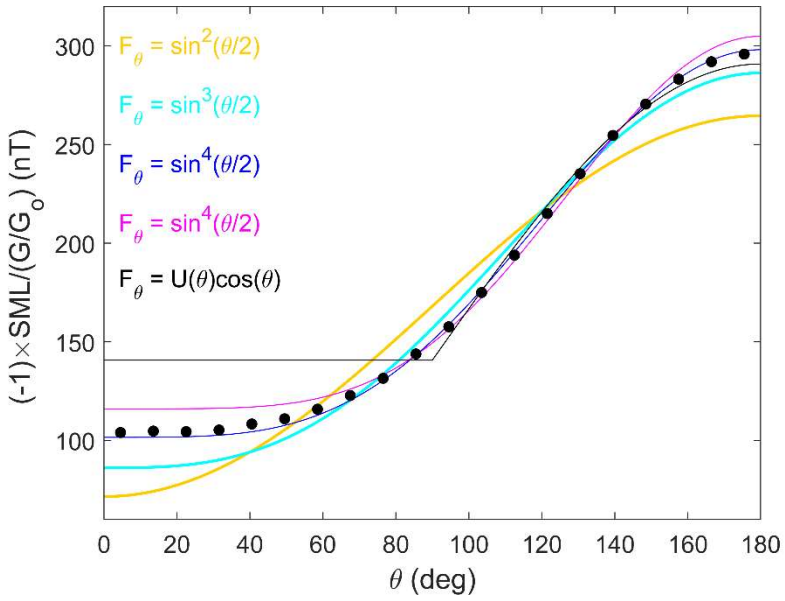

Figure S13. Same fits shown in Figures S7 –S11 bit shown on a $-SML/(G/G_o)$ versus θ axes. The data (black points) are the mean of the observed ratio $-SML/(G/G_o)$ in 9° wide bins of θ, and the IMF orientation factors are scaled to these data using the fits in Figures S7-S11 are, respectively: (orange) $\sin^2(\theta/2)$; (cyan) $\sin^3(\theta/2)$; (blue) $\sin^4(\theta/2)$; (mauve) $\sin^5(\theta/2)$; and (black) $U(\theta)\cos(\theta)$, where $U(\theta) = -1$ for $\theta \geq 90°$ and $U(\theta) = 0$ for $\theta < 90°$.

Part 4. Parts of Figure 8 of main text on an expanded scale

Figure 2g of the main paper reveals a peak in the occurrence of values of $R = \log_{10}(\langle F_\theta \rangle_{1min} / \langle F_\theta \rangle_{1yr}) \approx 0.45$ associated with IMF orientations close to southward (explained by the discussion of Figure 9 in the main text). This feature is off-scale in Figure 8(c) of main text which plots $\langle F_\theta \rangle_\tau / \langle F_\theta \rangle_{1yr}$ as a function of τ. Rather than expand the scale in Figure 8 of the main text and lose important detail in all panels, we here repeat Figures 8a and Figure 8c of main text on a y-axis doubled scale which enables us to see this feature and track its evolution with τ. Figure S14 is a re-plotting of parts (a) and (c) of Figure 8 of main text, with the expanded y axis and a slightly altered color scale to highlight the feature in F_θ at $\langle F_\theta \rangle_\tau / \langle F_\theta \rangle_{1yr} \approx 2.8$ and low τ.

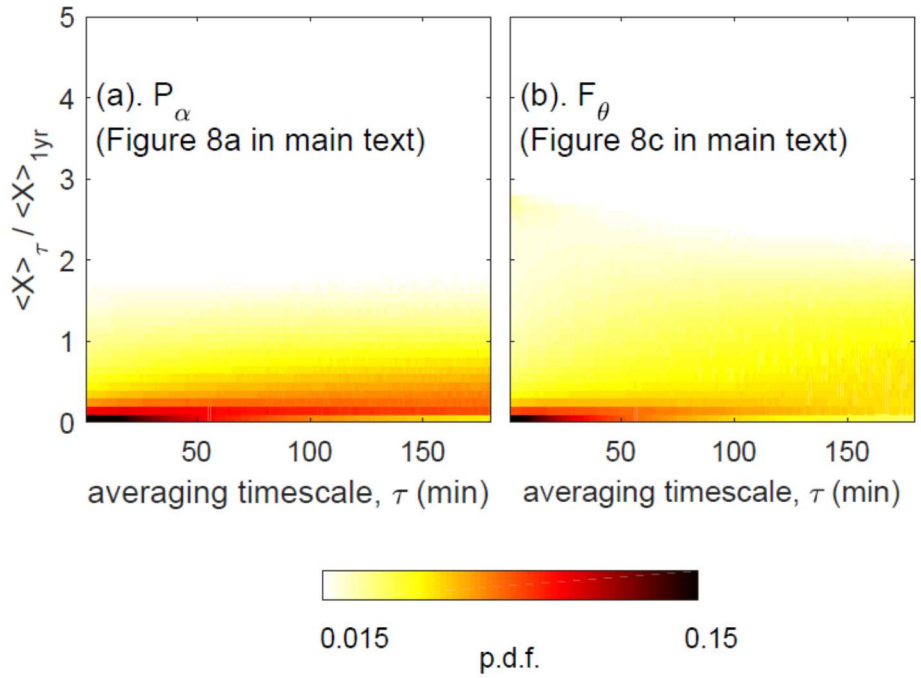

Figure S14. Parts (a) and (c) of Figure 8 of main text, here repeated on an expanded vertical scale (the panel height has been doubled to allow a y axis scale of double the length). Note the lower limit of the color axis has also been raised very slightly from 0 (used in main text) to 0.015 to help reveal the evolution of the feature in in F_θ at large $\langle F_\theta \rangle_\tau / \langle F_\theta \rangle_{1yr}$ and low τ.

Part 5 . Quantification of scatter in Figure 1 of main text

Figure 1 of the main paper gives scatter plots of the annual fractions of days when and index X exceeds X_o , its overall 95-percentile (for all available data), $f[X>X_o]$, as a function of its annual mean $\langle X\rangle_{\tau=1yr}$. The mauve lines in each panel are third-order polynomial fits to these data points , constrained to pass through the origin so that $f_{fit}[X>X_o]=0$ when $\langle X\rangle_{\tau=1yr}=0$ (i.e. the coefficient d is zero)

$$f_{fit}[X>X_o] = a\langle X\rangle_{\tau=1yr}^3 + b\langle X\rangle_{\tau=1yr}^2 + c\langle X\rangle_{\tau=1yr} + d \qquad \text{(S11)}$$

The fraction deviation of each point from the fitted line value is the evaluated

$$\Delta = (f_{fit}[X>X_o] - f[X>X_o]) / f[X>X_o] \qquad \text{(S12)}$$

For all non-zero values of $f[X>X_o]$ and the r.m.s. fractional fit residual computed, $\Delta_{rms} = \langle\Delta^2\rangle^{1/2}$.

The table below gives the coefficients, a, b, c, and d and the r.m.s. fractional fit residual computed, Δ_{rms} , for each of the geomagnetic indices shown in Figure 1 of the main text, plus for the normalized power into the magnetosphere, P_α/P_o and the normalized power without the IMF orientation factor, G_α/G_o (see equation S10). The rows are in rank order by the lowest scatter (i.e. in smaller Δ_{rms}).

rank	index	a	B	c	d	Δ_{rms}
1	AL	5.342×10^{-9}	4.521×10^{-6}	1.184×10^{-4}	0.000	0.1178
2	AE	-6.039×10^{-10}	1.670×10^{-6}	-8.107×10^{-5}	0.000	0.1384
3	AU	6.776×10^{-10}	1.036×10^{-6}	-2.211×10^{-4}	0.000	0.3412
4	G_α/G_o	-2.324×10^{-3}	9.056×10^{-2}	-4.734×10^{-2}	0.000	0.3780
5	Ap	-1.245×10^{-5}	7.583×10^{-4}	-4.200×10^{-3}	0.000	0.4337
6	P_α/P_o	-3.460×10^{-3}	1.447	-6.650×10^{-2}	0.000	0.7699
7	Dst	-3.134×10^{-6}	8.493×10^{-5}	-5.359×10^{-3}	0.000	1.1333